Int. J. Multiphase Flow Vol. 19, No. 1, pp. 151–172, 1993
Printed in Great Britain.

0301-9322/93 $6.00 + 0.00

SPACE–TIME EVOLUTION OF THE NONHOMOGENEOUS BUBBLE DISTRIBUTION IN UPWARD FLOW

I. ŽUN, I. KLJENAK and S. MOŽE
Faculty of Mechanical Engineering, University of Ljubljana, 61000 Ljubljana, Slovenia

(Received 14 July 1991; in revised form 26 October 1992)

Abstract—A two-dimensional computer simulation was developed to study the behavior of bubbles injected into a turbulent liquid stream in a vertical tube. The problem of scale separation was solved by a fully-interacting combination of a bubble segregation process, simulated in a Eulerian frame, and a bubble coalescence process, simulated in a Lagrangian frame. The interaction calculations were performed simultaneously and noniteratively. Fine-scale details were taken into account by assigning corresponding probabilities. For the first time, results of a simulation of void peak evolution from the wall region to the tube core are presented for vertical flow. Starting with randomly distributed bubbles, the processes of bubble segregation and bubble coalescence generate coherent structures of bubbles traveling upwards in the tube core in trains with basically the same characteristics as for slug flow, i.e. no lateral movement and periodic arrivals. Numerical calculations and a comparison with experimental data are given for some typical examples of wall void peaking and void coring flow regimes regarding three parameters: bubble structure, void fraction profiles and the power spectral density functions of the void fraction fluctuations.

Key Words: bubbly flow simulation, bubble segregation, bubble coalescence

INTRODUCTION

In spite of decades of experimental and theoretical research, knowledge of the different bubbly flow regimes and the related dynamical processes is still very limited. It seems that any real understanding of the nature of turbulent bubbly flow is not likely to be gained until more is known about the interaction of different structures. These structures may be recognized, for example, as bulk turbulent continuum properties, bubble wakes, single bubbles of various shapes and bubble–bubble structures. One of the macroscopic results of these interactions is the void fraction nonhomogeneous distribution in conduit flow. Parallel computing on different scales would probably lead to the solution of this problem, which at present remains unresolved. The reason for this lies in the potentially hazardous discrete modeling, because the length and time scales of the discretization in a multistructure picture always appear incompatible with the real system.

There have been several attempts to treat the problem of the bubbly-to-slug flow transition (BTS) in a less complex way. To a limited extent, they add an understanding of physics via certain parameters such as demarcation of the dominant flow patterns utilizing the probability density functions or power spectral density functions of the void fraction fluctuations (Jones & Zuber 1975), void fraction wave instabilities (Matuszkiewicz *et al.* 1987) etc. We believe, however, that if one wants to describe an evolutionary process, one must follow the dynamics of bubbly flow in a Lagrangian frame. Such a technique enables the study of microscale bubble interaction in order to understand the averaging scales. This paper represents a continuation of dynamic bubble flow simulation studies (Stuhmiller *et al.* 1983; Žun *et al.* 1988, 1991). In the model, bubbles of realistic shape may be located at any distance from the tube wall. The only limitation is the liquid laminar sublayer. Their interaction is based on the following principles: bubble transverse lift; bubble transverse dispersion; lateral penetration restraint to determine *bubble segregation*; and shear slip, wake drift and fluid–fluid interaction to determine the *bubble coalescence* process. Bubble train structures appear spontaneously as a result of the interaction of these phenomena, and are exhibited in void waves. The appearance of bubble coalescence within a particular bubble train structure is regarded as the onset of the bubbly-to-slug flow transition regime.

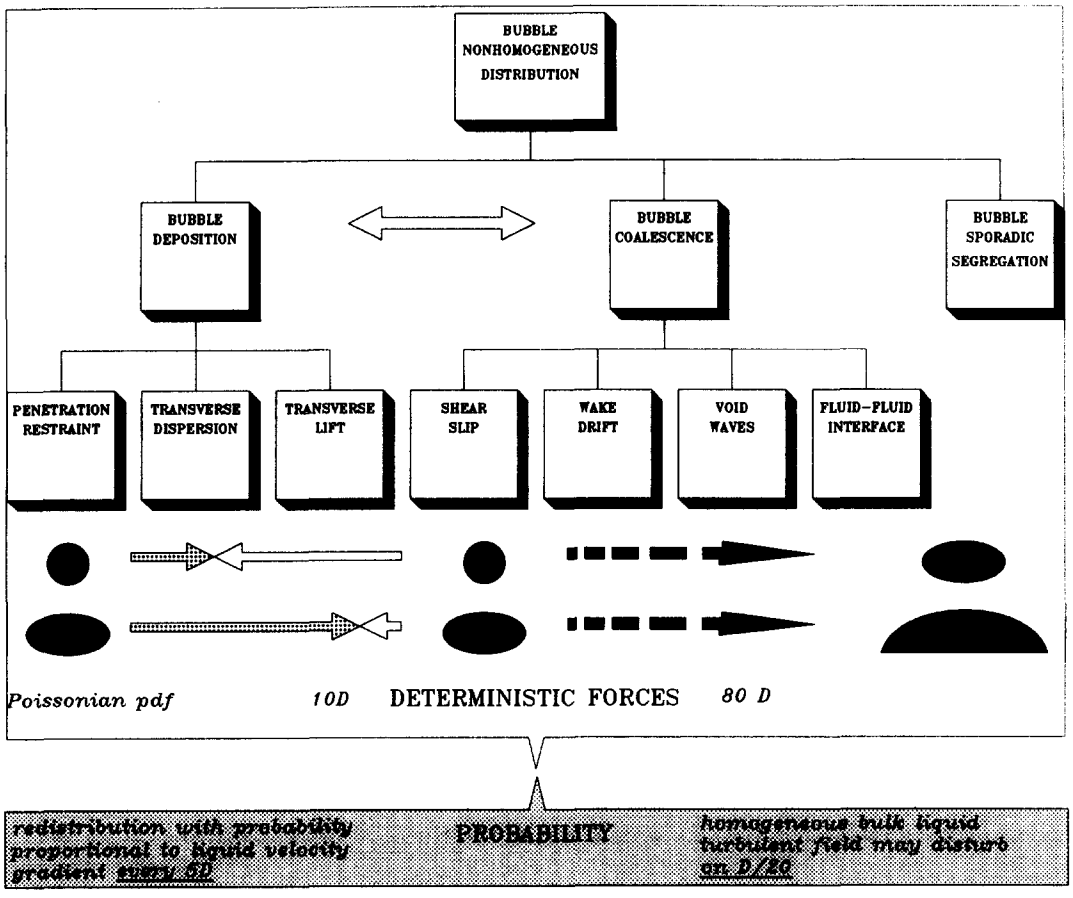

Figure 1. The primary principles of the bubble nonhomogeneous distribution in upward flow.

THEORY

Physical Picture

Nonhomogeneous, spatially random, distributed structures often tend to form periodic patterns. One example is turbulent, bubbly, upward flow, which in certain conditions changes its random structure into a periodic slug flow. One of the most intriguing questions in this context concerns the dynamics of evolution towards slugs. To answer the questions how and when each of these patterns takes place, a theory which deals with instability sharply localized in space and time is considered.

We postulate that the bubbly-to-slug flow transition is a deterministic phenomenon, although it evolves with time in a very complicated way, due to nonlinear interactions. The direct simulation of bubble movement (bubble tracking) is an attempt towards solving the problem deterministically. The simulation deals, however, only with large-scales flow, and contains errors due to our ignorance *vis-à-vis* the small scales, due to the lack of details concerning the initial, boundary and interfacial conditions and due to the inaccuracy of the numerical schemes. It follows that, even for a deterministic system, unpredictability and randomness must be introduced.

We believe that a nonhomogeneous void fraction radial distribution is a result of at least two simultaneous processes having different time scales: the first process is bubble deposition; the second is bubble coalescence. We combine our two earlier works on bubble deposition [or, in terms of the present work, massive segregation (Žun 1990)] and bubble coalescence (Žun *et al.* 1991) into a compound Eulerian/Lagrangian simulation. The two principal deterministic processes are shown in figure 1. Within the limits of our experiment, the bubble deposition took about $10D$ to reach a new equilibrium state, whereas the coalescence required about $80D$. In the case of a wall void

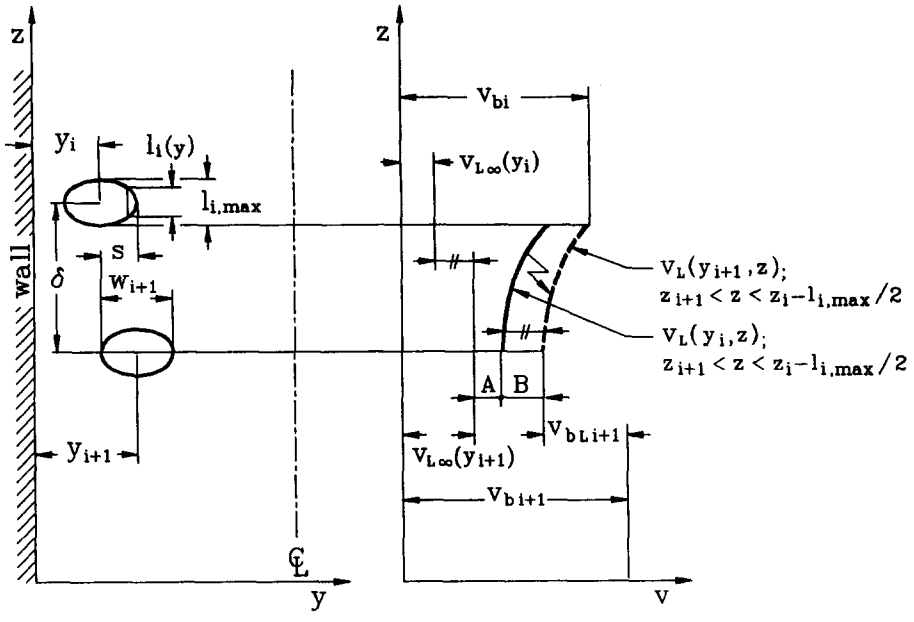

Figure 2. Interacting bubbles at the near wall; A—wake drift, B—shear slip.

peaking flow regime, it may therefore be expected that after bubble fusing the new larger bubbles would be redeposited (sporadic segregation) to the tube core. Because of insufficient information about the processes which take place on the bulk liquid turbulence scale we may talk about the uncertainty in the simulation of a possible outcome of bubble coalescence as well as bubble sporadic segregation. At the first stage of the approximation, to save on computer time and storage capacities, an homogeneous bulk liquid turbulent field was considered as a disturbance on a micro-scale which was taken within the limits of our experiment as $D/20$. Bubbles were redistributed according to local singularities defined by the deposition model every $5D$.

Bubble segregation

It was proved experimentally that in vertical upward polydispersed bubbly flow, bubbles with significant intrinsic helical motion tend to concentrate near the wall, while on the other hand, bubbles having weak intrinsic oscillatory motion tend to concentrate in the core region (Žun 1990). The corresponding void fraction profiles due to this massive segregation can be described by the bubble deposition model. According to this model, the bubble transverse penetration due to lift and diffusion correlates its intensity with the periodic structure of the bubble intrinsic motion; while on the other hand, large-scale turbulent eddies act as a restraining field to this penetration (Žun 1990). After coalescence takes place in the case of a wall void peaking flow regime, it may therefore be expected that larger bubbles would be redeposited (sporadically segregated) to the tube core which again can be predicted by the bubble deposition model. In the present simulation, bubble redeposition was limited by the presence of other bubbles. A necessary condition for a bubble to be laterally displaced was that no other bubble obstructed the motion. The probability of lateral displacement (p_d) to the neighboring radial coordinate (r) was taken as proportional to the undisturbed liquid velocity gradient:

$$p_d(r_{i+1}, r_i) = \frac{v_{L\infty}(r_i) - v_{L\infty}(r_{i+1})}{P_s}, \qquad [1]$$

where $v_{L\infty}$ is the undisturbed liquid velocity and P_s is a factor of bubble segregation.

The simulation incorporated a fully-interacting combination of the bubble sporadic segregation process by the aforementioned deposition model, simulated in a Eulerian frame, and a bubble coalescence process, simulated in a Lagrangian frame. The bubbles in the simulation tended to be redeposited according to their size, either because larger bubbles appeared as a result of expansion

and coalescence or because the bubbles' initial radial coordinates did not correspond to their deposition location.

Bubble coalescence

Shear slip. In general, bubbles of different shapes and sizes do not appear exactly centered in a radial position above each other, which results in nonuniform slip conditions at their interfaces. Those bubbles which are locally exposed to the higher liquid velocity region may therefore try to outrun the leading bubbles which are relatively more retarded by the wall region. This case is shown in figure 2. We call this effect *shear slip.*

Wake drift. The two-phase mixture is considered as fields: the undisturbed liquid away from the bubbles; the liquid disturbed by the bubbles; and the bubbles themselves. The bubble instantaneous velocity is the sum of the liquid velocity corresponding to the bubble center coordinate and the bubble relative velocity,

$$v_{bi}(t) = v_L(z_i, r_i, t) + v_{bLi}, \qquad [2]$$

where v_{bi} is the bubble relative velocity, v_L is the liquid velocity, z_i and r_i are the axial and radial coordinates of bubble i and t is the time. Away from bubbles, the undisturbed liquid velocity obeys the 1/7th power law:

$$v_{L\infty}(r) = v_{L\infty cl}\left(1 - \frac{r}{R}\right)^{1/7}, \qquad [3]$$

where $v_{L\infty cl}$ denotes the velocity at the tube centerline and R is the tube radius.

A trailing bubble is accelerated, relative to the leading bubble, due to the local increase in liquid velocity. The increased liquid velocity is described by wake perturbations in, basically, the same form as suggested by Bilicki & Kestin (1987):

$$v_L(z, r, t) = v_{L\infty}(r) + \left[\frac{l_{i,max}}{2(z_i - z)}\right]^{2\zeta/3}[v_{bi}(t) - v_{L\infty}(r_i)], \qquad [4]$$

where $l_{i,max}$ denotes the bubble maximum vertical chord length and ζ is the attenuation factor. As the velocity in the wake decreases with distance from the axis, the exponent $\zeta > 1$ was introduced to obtain a weaker wake drift.

Bubble interaction. The relative radial position of two bubbles is characterized by their *relative overlapping*, defined according to figure 2 as (Kljenak 1992):

$$s^* = \frac{s}{w_{i+1}}. \qquad [5]$$

The bubble velocity may be affected by the disturbed liquid according to [4], if the bubble relative overlapping of the two adjacent bubbles exceeds a limiting values s^*_{min},

$$s^* > {}^*_{min}. \qquad [6]$$

Bubble $i + 1$ then approaches bubble i, eventually collides and fuses with it. Otherwise, the bubble velocity follows [2] and [3] and bubbles i and $i + 1$ do not influence each other's motion. The simulation considers only bubble longitudinal collisions, whereas lateral collisions are not modeled.

The dependence of bubble interaction on their relative overlapping was investigated experimentally by Otake *et al.* (1977), who studied the coalescence of bubbles in swarms. According to them, coalescence takes place when more than about a half of the projected area of the following bubble overlaps with that of the leading bubble. The minimum relative overlapping necessary for bubble interaction also accounts for the influence of bubble lateral oscillations, due to liquid turbulence. These oscillations may cause aligned bubbles to overtake one another without colliding.

Bubble train structure. A group of bubbles forms a so-called train if the vertical distance between the centers of successive bubbles is less than a prescribed value δ_{max} and if their relative overlapping is greater than s^*_{min}. The relative overlapping behind a bubble i in a train is defined as

$$s^* = \frac{k_{ti}s}{w_{i+1}}, \qquad [7]$$

where w is the bubble width. According to [7] the possibility of bubble train growth in the lateral direction increases with an increasing number of bubbles. It is also assumed that a bubble train causes a stronger wake drift than a single bubble. The liquid velocity behind bubble i is weighted by k_{ti} at the bubble maximum vertical chord $l_{i,\max}$:

$$v_L(z, r, t) = v_{L\infty}(r) + \left[\frac{k_{ti} l_{i,\max}}{2(z_i - z) + (k_{ti} - 1) l_{i,\max}}\right]^{2\zeta/3} [v_{bi}(t) - v_{L\infty}(r_i)]. \quad [8]$$

The bubble train concept is based on the assumption that bubbles which are sufficiently close together may act as a single entity and cause stronger disturbances in their vicinity than a single bubble. This effect has been noticed by Tsuchiya *et al.* (1989) in studies of fluidized beds. It is assumed that disturbances do not build up indefinitely: their sum reaches a maximum value after a few bubbles have gathered.

Fusion of bubbles. After collision, bubbles stick and move together for the period of so-called rest time before they fuse into a larger resulting bubble, except near the wall where fusion is instantaneous. The wall region is fixed by the nearest possible radial coordinate.

After fusion, to define new coordinates for the resulting bubble, a volume weighted mean of the corresponding coordinates of each particular bubble just before fusion is considered.

Turbulent breakup of bubble clusters. Bubble interaction may be disturbed by dispersion due to wall-generated liquid turbulence and vortex shedding of the leading bubble. If bubble $i + 1$ trails bubble i, trailing may be disrupted with a probability p_t to behave as if condition [6] is not satisfied until bubble $i + 1$ has moved a distance of l_t.

The liquid disturbances may also disperse the sticking bubbles in reality, which was simplified in the model by resetting the rest time to zero, except in the wall region.

The role of turbulent dispersion forces in the prevention of the bubble coalescence process is discussed in Prince & Blanch (1990) and Thomas (1981). Turbulent fluctuations may bring bubbles together or move them apart. They can also cause bubble breakup, which is not explicitly included in the present model.

Time scales. The process of bubble coalescence is therefore considered to have three time scales (figure 1): the first is a result of shear slip; the second follows [4] or [8], which we name wake drift; and the third is defined empirically from experiments to account for the thinning of the liquid film between two bubbles sticking together. This is the time when the bubble appears to rest on the predecessor's interface before the fusion process. In the wall region, bubble fusion is assumed to occur instantaneously after collision because of the large difference in bubble velocities.

Numerics

Bubbles were assumed to be rigid elements moving vertically upwards in a tube (figure 3). The flow was homogeneous in the azimuthal direction and symmetric relative to the $\theta = \pi/2$ plane. The position of bubble i was defined by the coordinates (z_i, r_i, θ_i) of its center. Bubbles had different shapes: ellipsoidal, spherical cap and bullet slug (Kljenak & Žun 1991). Bubbles entering the tube were initially ellipsoids. Spherical caps and gas slugs were formed by coalescence and expansion due to pressure drop. Ellipsoids could be located anywhere within the tube cross section, whereas spherical caps and slugs were always at the tube centerline (Žun 1990).

Only those bubbles which intersected the $(0 \leqslant z, 0 \leqslant r \leqslant R, \theta = 0)$ plane, and were initially centered in the observed half of the tube, were tracked in the simulation. An example of cross-sectional grid points where bubble centers could be located is shown in figure 4. The area covered by the numerical grid depended on the initial bubble size. The numerics are described in detail in Kljenak & Žun (1991) and Kljenak (1992).

As the flow was assumed axisymmetric, a "mirror" process was considered on the $(0 \leqslant z, 0 \leqslant r \leqslant R, \theta = \pi)$ plane. If a bubble extended across the tube axis, a part of a counterpart bubble from $(0 \leqslant z, 0 \leqslant r \leqslant R, \theta = \pi)$ was therefore taken into account in the void fraction calculation and in the correction algorithm which modeled three-dimensional effects (figure 3).

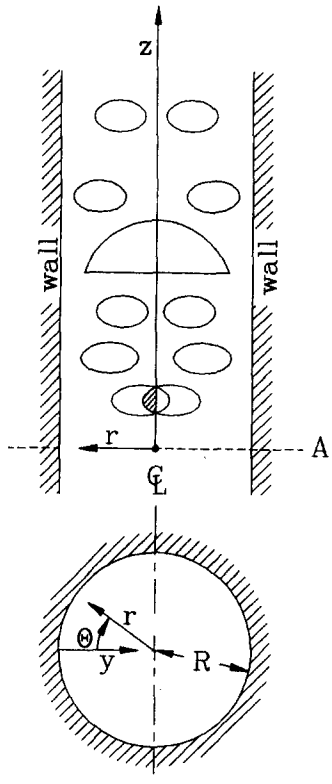

Figure 3. Coordinate system of bubbly flow in the experimental test section.

Gas-phase conservation

An instant void fraction ϵ in the entire tube was determined from

$$\epsilon = \frac{\sum_i \int_{y_i - w_i/2}^{y_i + w_i/2} l_i(y) 2\pi (R - y)\, \mathrm{d}y}{\pi R^2 L} = \frac{\sum_i I_i}{\pi R^2 L}, \qquad [9]$$

where $l_i(y)$ denotes the bubble vertical chord length in the $(0 \leqslant z, 0 \leqslant r \leqslant R, \theta = 0)$ plane and the summation extends over all bubbles in the simulation. A correction algorithm was used for the sum of integrals I_i to ensure void fraction conservation. $\Sigma_i I_i$ must remain constant over a large number of bubble fusions and bubble lateral displacements.

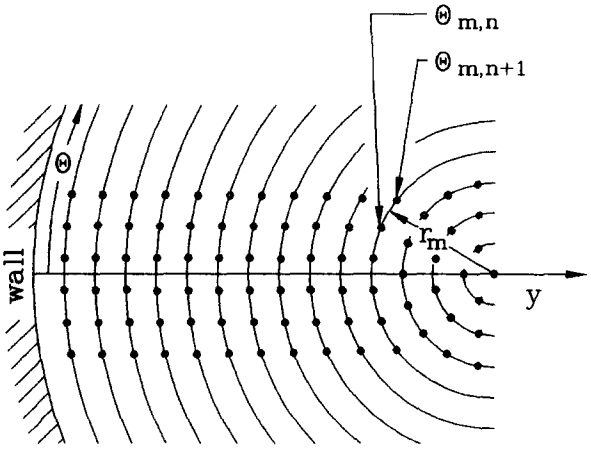

Figure 4. An example of cross-sectional discrete coordinates.

In an earlier version of the simulation, this was achieved by increasing the bubble size accordingly after lateral displacement or fusion. The details are given in Kljenak & Žun (1991). The increase in the bubble volume accounted for instant coalescence with bubbles coming from a nontracked bubble population.

In the present version, where the influence of the liquid phase turbulence on bubble interaction was taken into account, it was assumed that the turbulence may prevent bubbles from coalescing. Therefore, the conservation of the sum of intergrals I_i was achieved either by increasing the bubble volume after lateral displacement or fusion or by generating additional identical bubbles at the same cross-sectional location. The generation of additional bubbles accounted for the displacement of bubbles from nontracked tube regions. At each bubble lateral displacement or fusion, additional bubbles were generated with probability p_t, whereas the bubble volume was increased with probability $1 - p_t$.

Bubble sporadic segregation

If a bubble had to be displaced laterally from a coordinate r_i to a coordinate r_j, the probability of displacement was considered for each partial displacement from r_k to r_{k-1}, $j < k \leqslant i$. A newly formed spherical cap bubble was displaced instantly to the tube centerline.

Bubble redeposition was modeled as instantaneous lateral displacement. Each bubble was eventually redeposited after having moved axially a distance of $5D$.

Bubble motion

Bubble movement was calculated with a discrete time-step method. The bubble axial coordinate at time $t + \Delta t$ follows from

$$z_i(t + \Delta t) = z_i(t) + v_{bi}(t)\,\Delta t. \qquad [10]$$

Assumptions

Initial and boundary conditions

Experimental results of the void fraction distribution at position A were used as the initial condition for the simulation; $z = 0$ at level A. A Poissonian distribution of time intervals between bubble generations was prescribed to create a random process. Bubbles were generated randomly to simulate both void fraction profiles and the PSDF (power spectral density function) of the void fraction fluctuations either at $z = 0$ or $z = -33D$. The latter case was used to create a PSDF which showed an onset of periodicity already at level A because of different mixing conditions.

The probability density function (pdf) of the bubble initial radial coordinate was calculated by a trial-and-error procedure from the measured void fraction profile at level A. It was composed of a set of discrete values, corresponding to discrete radial coordinates. There were some minor difficulties in obtaining a perfect fit because of the constraints in the model: quasi-3D picture; mirror process in the other half of the tube; constant bubble size or only two values; and discrete cross-sectional coordinates.

In the case of the wall void peaking flow regime, smaller bubbles were generated near the wall to obtain the same initial void fraction profile as in the experiment. The smaller bubble diameter had to be taken because of the unrealistic simulation with a fixed horizontal position of the bubbles' major axis. Here, a further step should be taken in the future towards prediction of the bubbles' major axis inclination angle.

The bubble relative velocity in [2] was defined as the difference between the bubble absolute velocity and the local liquid velocity corresonding to the bubble center coordinates. This slip was termed to equal terminal speed and was calculated from a correlation by Wallis (1975). The effect of liquid turbulence on the bubble drag was therefore neglected.

Ellipsoidal bubbles and spherical caps were also distinguished as by Wallis (1975). Ratios between the major and minor axis for ellipsoidal bubbles were calculated by a correlation by Kubota (Serizawa 1974). As a first approximation, an isothermal expansion of bubbles during the upward flow was assumed. We are aware that this might be far from reality in the developing region where a mechanical nonequilibrium due to mixing prevails.

Inertial effects were neglected. A homogeneous, isotropic bulk liquid turbulent field was assumed.

Bubble sporadic segregation

The same coefficients were used as in Žun (1990) for the bubble deposition model. Two values were taken for P_s in [1]: for $\langle \epsilon \rangle \leqslant 0.025$, P_s was set equal to 0.015, whereas for $\langle \epsilon \rangle \geqslant 0.040$, P_s was equal to 2.0.

Bubble coalescence

The value used for Δt was 1.2 ms for $j_L = 1.00$ m/s and 2.4 ms for $j_L = 0.45$ m/s. The bubble rest time was set equal to 2.5 s. ζ in [4] and [8] was taken as 3.0, as in the earlier version of the model.

The value of the minimum relative overlapping necessary for bubble interaction was $s^*_{min} = 0.2$. In the earlier version of the model (Žun *et al.* 1991), the value 0.3 was used instead because only bubbles with centers situated in the $(0 \leqslant z, 0 \leqslant r \leqslant R, \theta = 0)$ plane were tracked in the simulation. As the bubbles obstruct each other less in this new version of bubble tracing in a segment of the (z, r, θ) space, a weaker criterion has been set for their interaction. Otherwise, bubbles move independently of each other. In addition to this, the distance δ_{max} was taken as twice the maximum vertical chord length of the leading bubble. It was assumed that the effects of individual bubbles in the train are simply added:

$$k_{ti} = \sum_{j=i-3}^{i} n_{bj}, \qquad [11]$$

where n_{bj} denotes the impact of bubble j; n_{bj} was chosen as 1 for ellipsoidal bubbles and as 2 for spherical cap bubbles and gas slugs. k_{ti} was limited by 4. It was further assumed that spherical cap bubbles and gas slugs are not affected by the wake drift of ellipsoidal bubbles.

The influence of the liquid turbulence on bubble interaction was considered at each time step. Bubbles which were interacting through the wake effect did not influence each other's motion, whereas in the case of sticking bubbles the sticking time was reset to 0. In both cases, a corresponding probability of turbulence impact was measured by the probability of turbulent dispersion p_t for every time sequence related to $l_t = D/20$. Two values were used for p_t; for $j_L = 0.45$ m/s, p_t was equal to 0.05, whereas for $j_L = 1.00$ m/s, p_t was equal to 0.75. This value did not prevent the transition from a random towards a periodic structure at higher void fraction values.

3. EXPERIMENT

Figure 5 shows the experimental setup schematically, with a vertical test section. The test section was made from a transparent square channel 30 × 30 × 4680 mm, the same as in earlier studies (Žun *et al.* 1991). The entrance and exit consisted of expansions into plenum areas. To reduce secondary flow, spheres of 10 mm dia were packed into the inlet plenum. The loop could have been open or closed. In this paper, the results for the open run of filtered tap water are given. The reason we chose an open run is because we wanted to avoid any periodic noise from the water pump. The water volumetric flux was 0.45 and 1.00 m/s, which corresponds to bulk water Reynolds numbers of approx. 13,400 and 29,800, respectively. A single bubble generator was centered in the test section $10D$ downstream from the inlet plenum to suspend uniform bubbles. For roughly the same bubble size, the average void fraction was increased by increasing the number of nozzles (of constant diameters) of generator.

The input measuring location was 1 cm downstream from the bubble generator. Here, the frequency of bubble generation was measured when a single nozzle was in operation. Output measuring locations A, B and C were chosen sequentially, at a distance of $\sim 40D$. At each output location absolute pressure and differential pressure were measured. Void fraction profiles in the

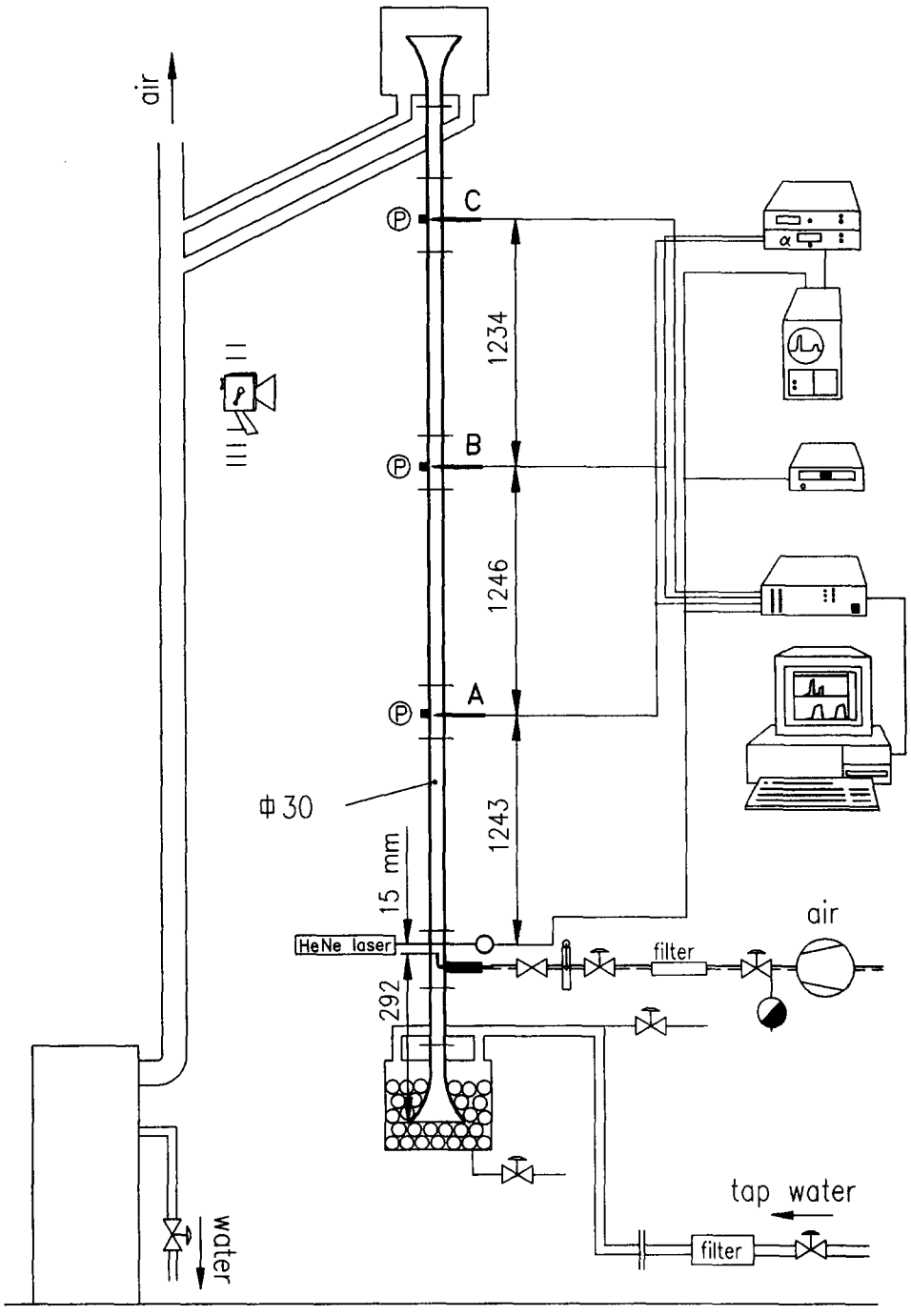

Figure 5. Schematic of the experimental setup.

radial direction and the PSDF at the tube centerline were obtained from signals given by resistivity micro-probes of 0.011 mm tip diameter. To avoid probe intrusion effects, only one profile was measured at a time. There was an on-line analysis of the data by an c-meter similar to a type produced commercially by DISA. An off-line analysis of the digitized probe data was carried out on each set of measurements. A camera, run by a motor, provided a large series of photographs of bubble structure at each level. When possible, the photographs were analyzed by digital image processing to obtain bubble structure statistics. The air flow rate was measured and controlled by either standard flowmeters or MKS meters, and the water flow rate was controlled by a calibrated orifice.

4. COMPARISON OF THE SIMULATION WITH EXPERIMENTAL RESULTS

A set of measurements was carried out at liquid volumetric fluxes of 0.45 and 1.00 m/s for the average bubble size range of 3–7 mm at level A. The sampling frequency for experimental and predicted PSDFs was chosen as 409.6 Hz for $j_L = 0.45$ m/s and as 819.2 Hz for $j_L = 1.00$ m/s. PSDFs were calculated over 128 samples, each containing 4096 points. A comparison of the simulated and experimental data shows consistency in the evolution of the void fraction profiles as well as in the transition from random into "periodic" bubbly structures. The following figures provide some examples characteristic of the transition from wall void peaking to void coring or void coring evolution at $j_L = 1.00$ m/s and one example of a void wall peaking flow regime simulation at $j_L = 0.45$ m/s.

An example of the prediction of void fraction profiles for a wall void peaking bubbly flow regime is shown in figure 6 for $j_L = 0.45$ m/s and $\langle \epsilon \rangle_A = 0.5\%$. The void fraction slightly increases in the core region at level C due to sporadic bubble coalescence and the resulting segregation. The characteristics of bubble arrivals were Poissonian at all levels in the experimental and simulated run. The calculated average bubble equivalent sphere diameter (d_{be}) was 3.95 mm. The probability of turbulent dispersion p_t was set as 0.05 and the factor of bubble segregation P_s as 0.015.

An example of bubbly flow structure for $j_L = 1.00$ m/s and $\langle \epsilon \rangle_A = 4.8\%$ is shown in figure 7a. The void fraction increases at level C in the core region to a magnitude characteristic of an intermediate profile in both the experimental and simulated runs (figure 7b). The magnitude of the void fraction increase in the tube core is reasonably good in comparison with the experimental results. The discrepancies stem from the assumption of an homogeneous bulk liquid turbulent field. A comparison of figures 7c and 7d shows that the contribution of the wake drift to bubble coalescence is negligible in comparison with the shear slip. The characteristics of bubble arrivals were Poissonian at all levels in both the experimental and simulated runs, figure 7e. From photographs, the calculated d_{be} was 4.70 mm. The d_{be} at level A was set as 4.70 and 3.60 mm at the near wall. The comparison of the evolution of the d_{be} distribution from A to C for the experimental and simulated runs is shown in figure 7f. The contribution of bubble coalescence in the experimental run is comparable with the simulated one. We are aware that the simulated distributions are not realistic in their details. However, to make a modeling of bubble size distributions sound, two problems have to be solved first, i.e. simulation of bubble mixing and bubble wobbling. The probability of turbulent dispersion p_t was set as 0.75 and the factor of bubble segregation P_s as 2.0.

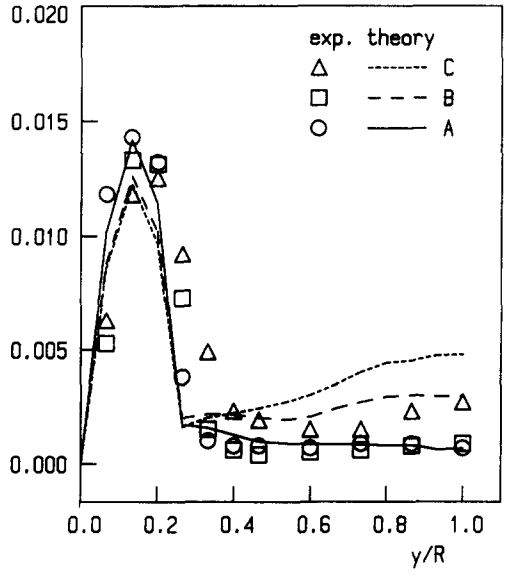

Figure 6. Experimental and predicted void fraction profiles; $j_L = 0.45$ m/s, $\langle \epsilon \rangle_A = 0.005$.

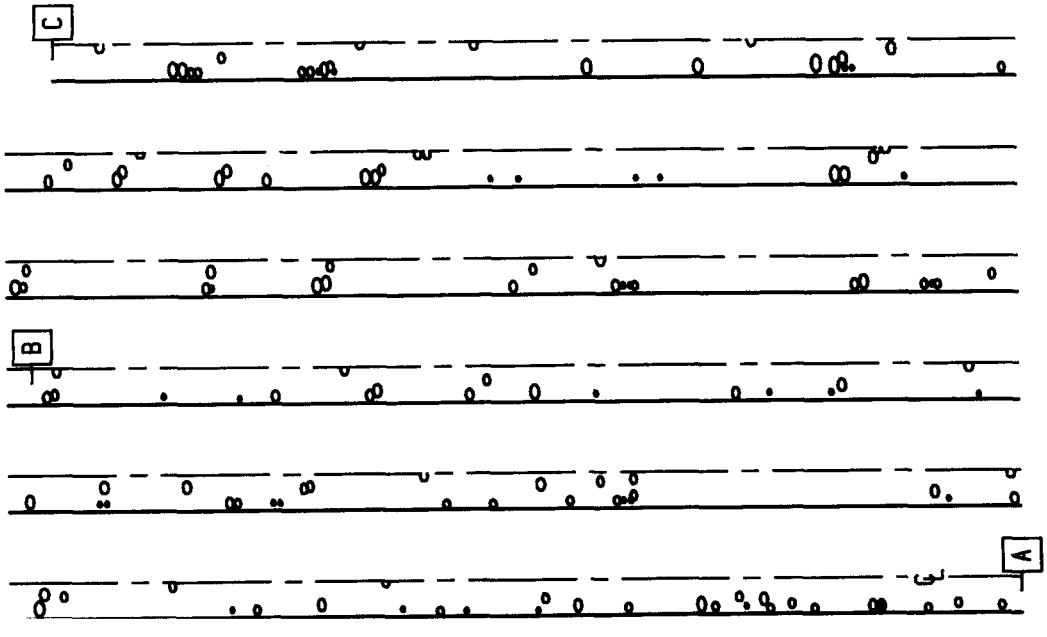

Figure 7a. An example of an instantaneous picture of the simulated flow; $j_L = 1.00$ m/s, $\langle \epsilon \rangle_A = 0.048$.

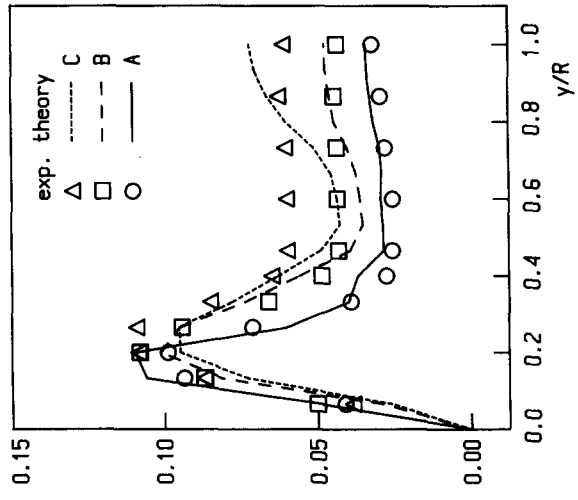

Figure 7b. Experimental and predicted void fraction profiles; $j_L = 1.00$ m/s, $\langle \epsilon \rangle_A = 0.048$.

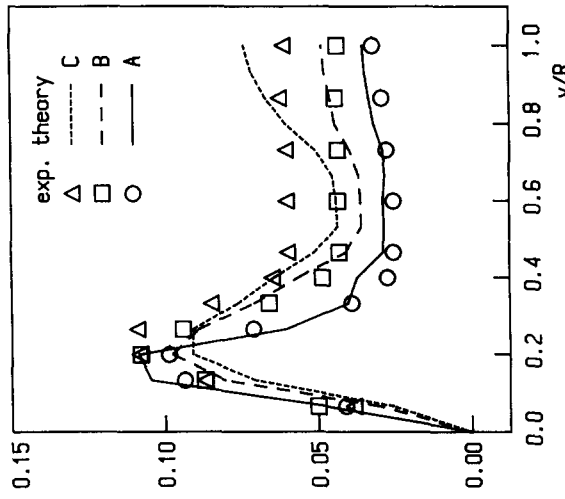

Figure 7c. Experimental and predicted void fraction profiles; *no wake drift*, $j_L = 1.00$ m/s, $\langle \epsilon \rangle_A = 0.048$.

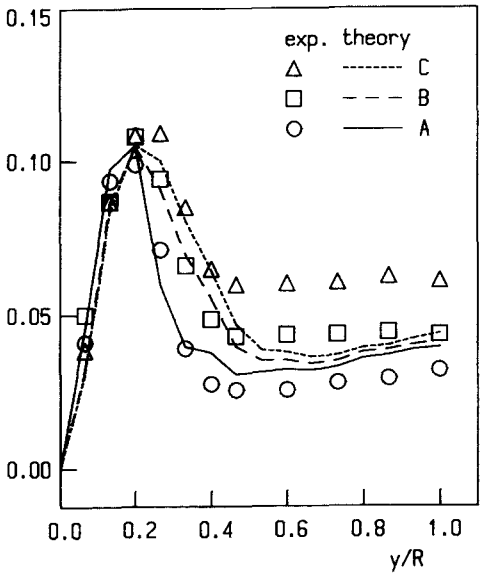

Figure 7d. Experimental and predicted void fraction profiles; *no shear slip*, $j_L = 1.00$ m/s, $\langle \epsilon \rangle_A = 0.048$.

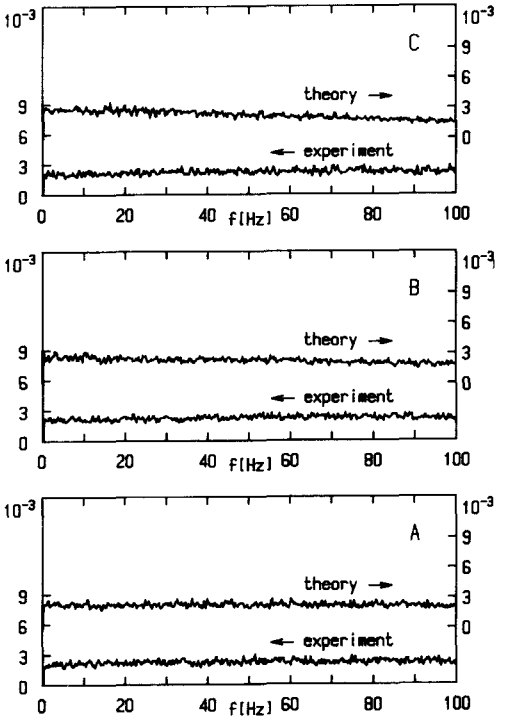

Figure 7e. Experimental and predicted PSDFs; $j_L = 1.00$ m/s, $\langle \epsilon \rangle_A = 0.048$.

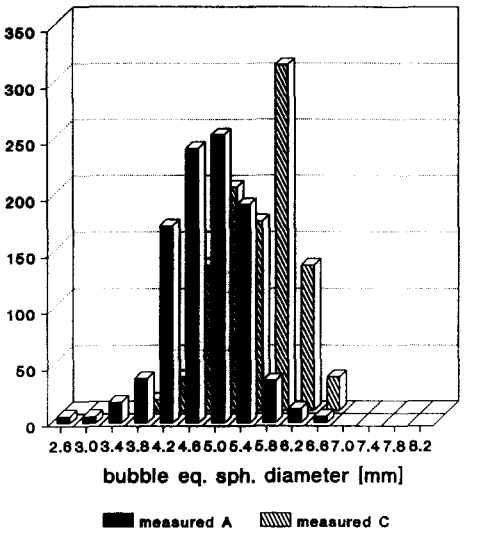

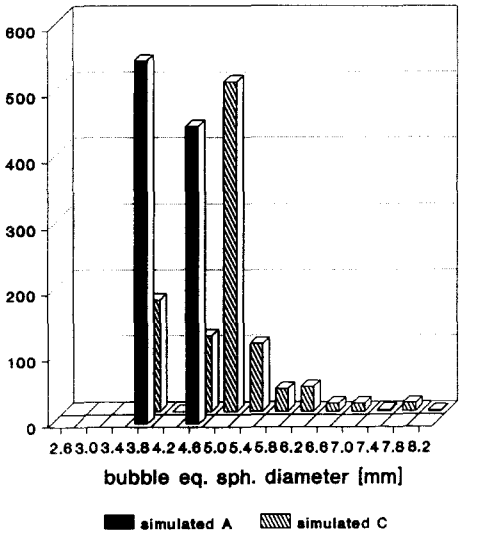

Figure 7f. Evolution of d_{bc} distributions; $j_L = 1.00$ m/s, $\langle \epsilon \rangle_A = 0.048$.

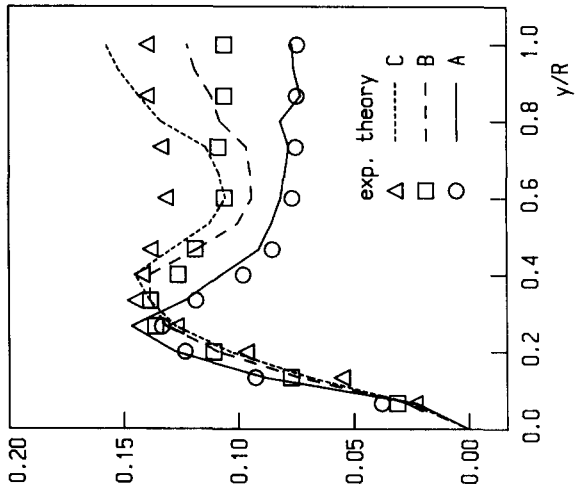

Figure 8b. Experimental and predicted void fraction profiles; $j_L = 1.00$ m/s, $\langle \epsilon \rangle_A = 0.085$.

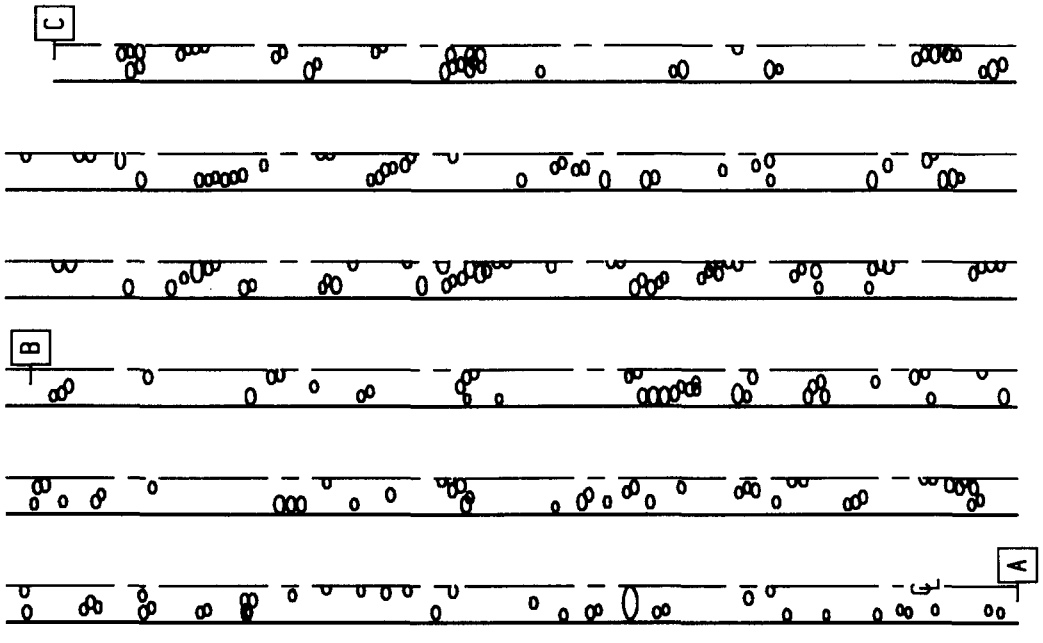

Figure 8a. An example of an instantaneous picture of the simulated flow; $j_L = 1.00$ m/s, $\langle \epsilon \rangle_A = 0.085$.

An example of bubbly flow structure for $j_L = 1.00$ m/s and $\langle \epsilon \rangle_A = 4.8\%$ is shown in figure 7a. The void fraction increases at level C in the core region to a magnitude characteristic of an intermediate profile in both the experimental and simulated runs (figure 7b). The magnitude of the void fraction increase in the tube core is reasonably good in comparison with the experimental results. The discrepancies stem from the assumption of an homogeneous bulk liquid turbulent field. A comparison of figures 7c and 7d shows that the contribution of the wake drift to bubble coalescence is negligible in comparison with the shear slip. The characteristics of bubble arrivals were Poissonian at all levels in both the experimental and simulated runs, figure 7e. From photographs, the calculated d_{bc} was 4.70 mm. The d_{bc} at level A was set as 4.70 and 3.60 mm at the near wall. The comparison of the evolution of the d_{bc} distribution from A to C for the experimental and simulated runs is shown in figure 7f. The contribution of bubble coalescence in the experimental run is comparable with the simulated one. We are aware that the simulated distributions are not realistic in their details. However, to make a modeling of bubble size distributions sound, two problems have to be solved first, i.e. simulation of bubble mixing and bubble wobbling. The probability of turbulent dispersion p_t was set as 0.75 and the factor of bubble segregation P_s as 2.0.

An example of bubbly flow structure is shown in figure 8a for $j_L = 1.00$ m/s and $\langle \epsilon \rangle_A = 8.5\%$. A more profound tendency towards an intermediate void fraction profile can be seen in figure 8b.

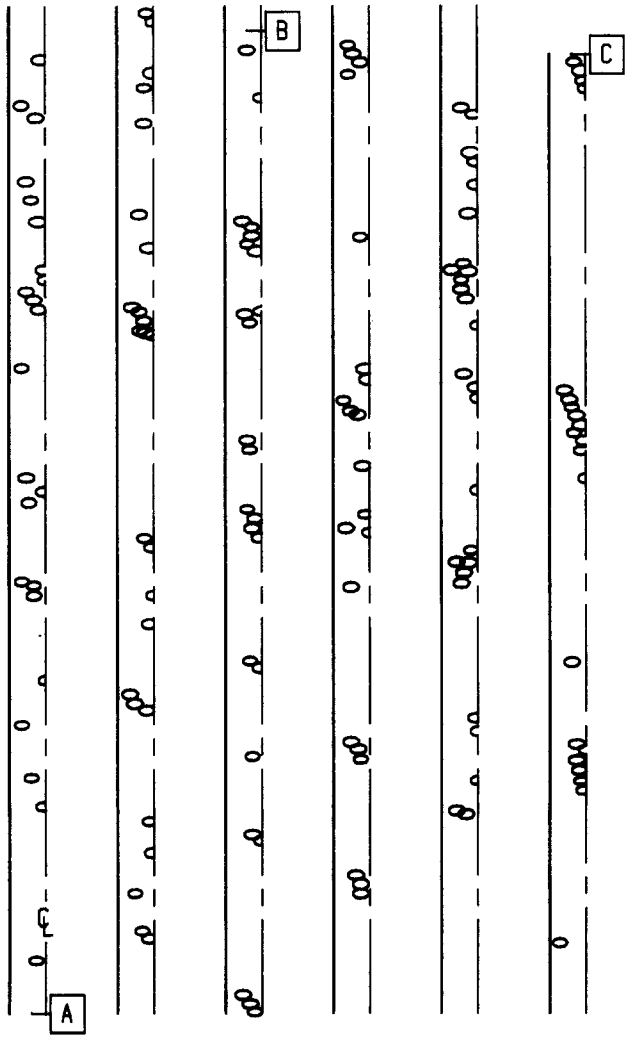

Figure 9a. An example of an instantaneous picture of the simulated flow; $j_L = 1.00$ m/s, $\langle \epsilon \rangle_A = 0.040$.

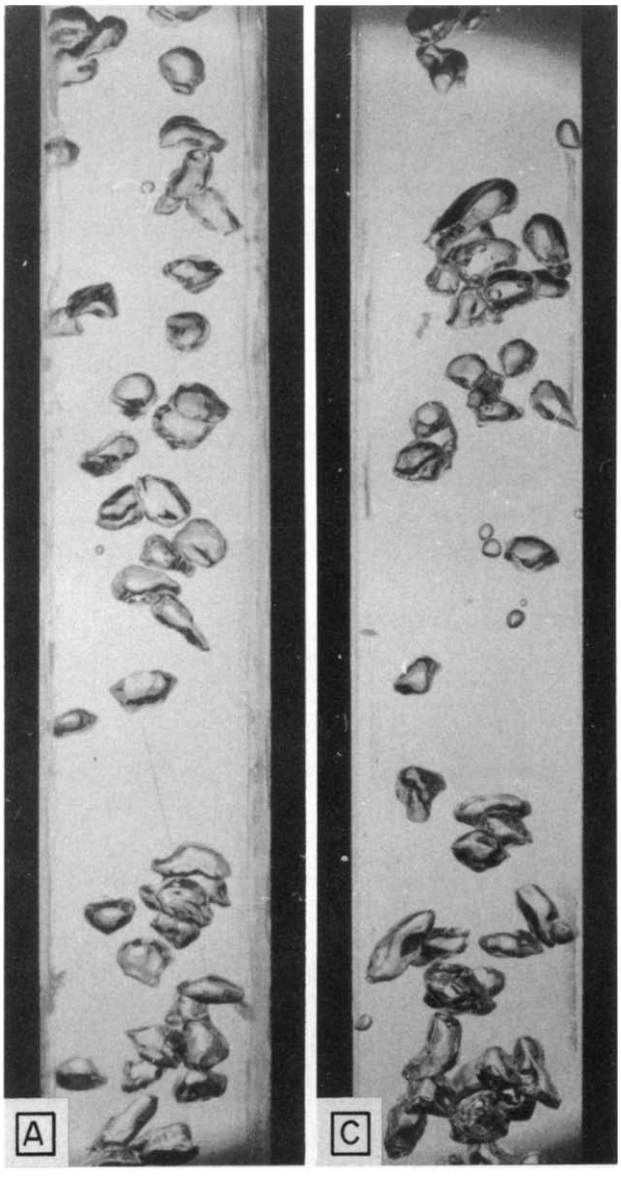

Figure 9b. An example of photo-shots at levels A and C; $j_L = 1.00$ m/s, $\langle \epsilon \rangle_A = 0.040$.

PSDFs still had random characteristics similar to those in figure 7e. From photographs, the calculated d_{be} was 5.00 mm. The d_{be} was set as 5.00 and 4.50 mm at the near wall. The probability of turbulent dispersion p_t was again set as 0.75 and the factor of bubble segregation P_s as 2.0.

An example of bubbly flow structure for $j_L = 1.00$ m/s and approximately the same average void fraction as in figure 7a, $\langle \epsilon \rangle_A = 4.0\%$, but larger bubbles, d_{be} calculated from photographs was 5.80 mm, is shown in figure 9a. The grouping of bubbles into "coherent" structures with a tendency to periodic appearance is shown in a photograph taken at level A, and the tendency towards sporadic coalescence in a photograph taken at level C (figure 9b). The corresponding experimental and predicted normalized PSDFs are shown in figure 9c. From this figure the transition from a random to periodic appearance of the bubble structures may be seen as quantitative data. The agreement between the experimental data and the simulation was extremely good. Measured and predicted void fraction profile evolutions from A to C are shown in figure 9d. Again, a good agreement between the experimental and theoretical results was obtained. The d_{be} diameter was initially set over the whole tube cross section at the value obtained from photographs. The probability of turbulent dispersion p_t was again set as 0.75 and the factor of bubble segregation P_s as 2.0.

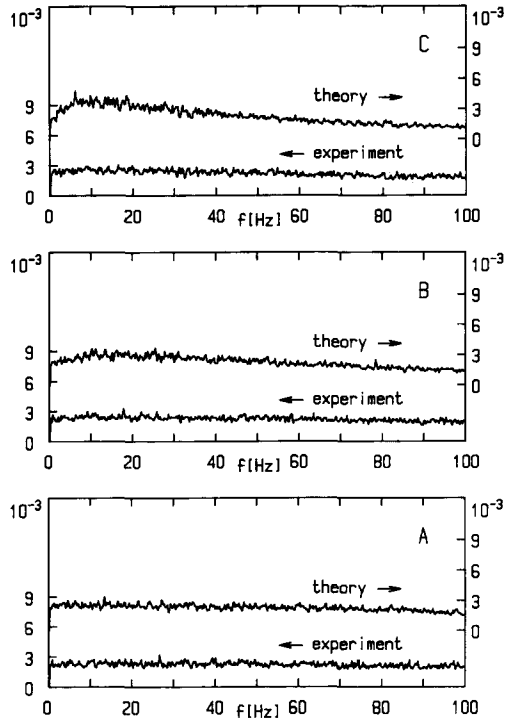

Figure 9c. Experimental and predicted PSDFs; $j_L = 1.00$ m/s, $\langle \epsilon \rangle_A = 0.040$.

Finally, an example of bubbly flow structure for $j_L = 1.00$ m/s and the same average void fraction as in figure 8a, $\langle \epsilon \rangle_A = 8.5\%$, but larger bubbles, d_{be} was estimated as 6.00 mm, is shown in figure 10a. For comparison, corresponding examples of photographs are given in figure 10b. This run highlights the important role of the bubble injection mechanism. Here, $33D$ of additional channel was used to create a bubbly flow structure from a Poissonian to the one observed in the test section at level A. From this figure so-called train structures in the $(0 \leqslant z, 0 \leqslant r \leqslant R, \theta = 0)$ plane can be identified. The corresponding experimental and predicted normalized PSDFs are shown in figure

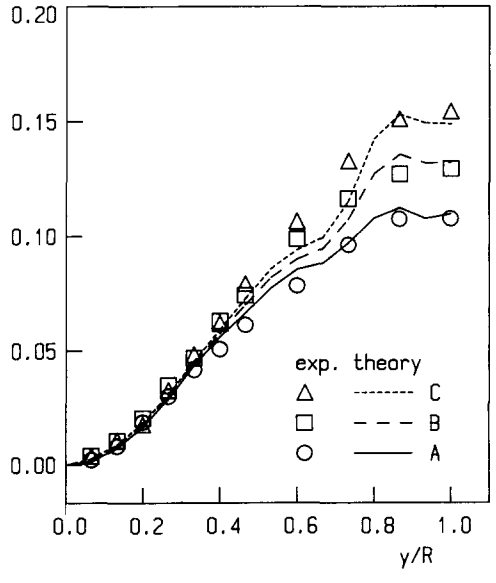

Figure 9d. Experimental and predicted void fraction profiles; $j_L = 1.00$ m/s, $\langle \epsilon \rangle_A = 0.040$.

10c. Again, the agreement between the experimental data and the simulation was extremely good. Comparison of figures 10d and 10e again points out that the contribution of the wake drift to bubble coalescence is negligible in comparison with the shear slip. A measured and predicted void fraction profile evolution from A to C is shown in figure 10f. The d_{be} was initially set at an estimated value over the whole tube cross-section. The probability of turbulent dispersion p_t was again set as 0.75 and the factor of bubble segregation P_s as 2.0.

5. DISCUSSION

The physical picture adopted in this work recognizes basically three different scale domains. The largest one is determined by the time needed for the evolution from a "dispersed bubble structure", characterized by an almost constant PSDF of the void fraction fluctuations, to "bubble swarm (train) structures", characterized by the peaking of the PSDF at characteristic frequencies which may be regarded as the onset of slugging. The intermediate scale domain is defined by the time needed for bubbles of a particular size to reach preferable radial locations in a turbulent liquid shear flow. Omitted fine-scale details due to the turbulent liquid field and interfacial nonequilibrium give us cause to assign only the probability of an outcome defined on an intermediate scale. This

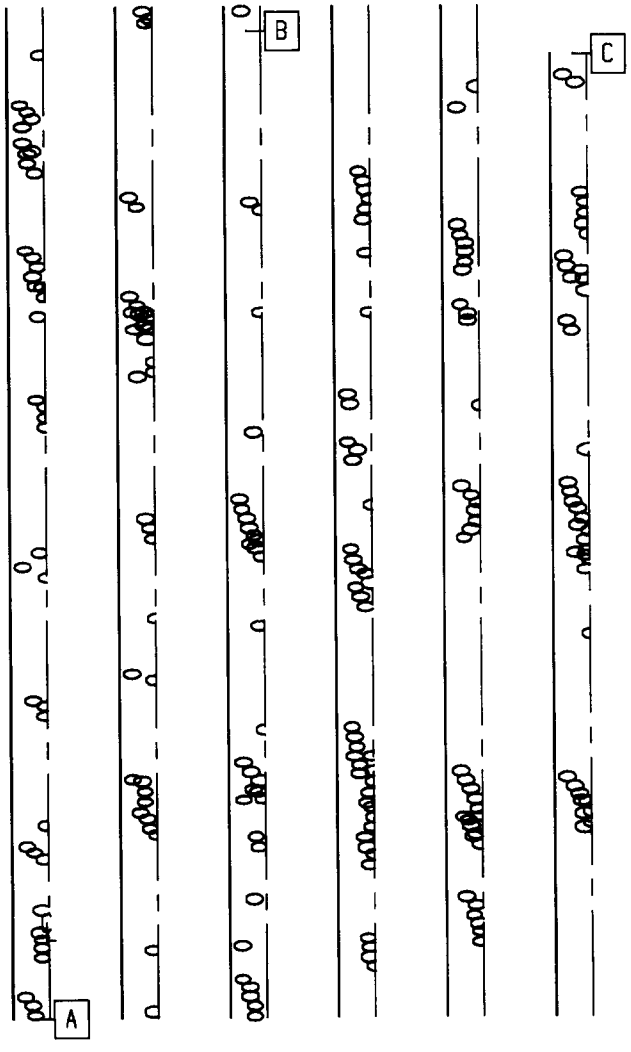

Figure 10a. An example of an instantaneous picture of the simulated flow; $j_L = 1.00$ m/s, $\langle \epsilon \rangle_A = 0.085$.

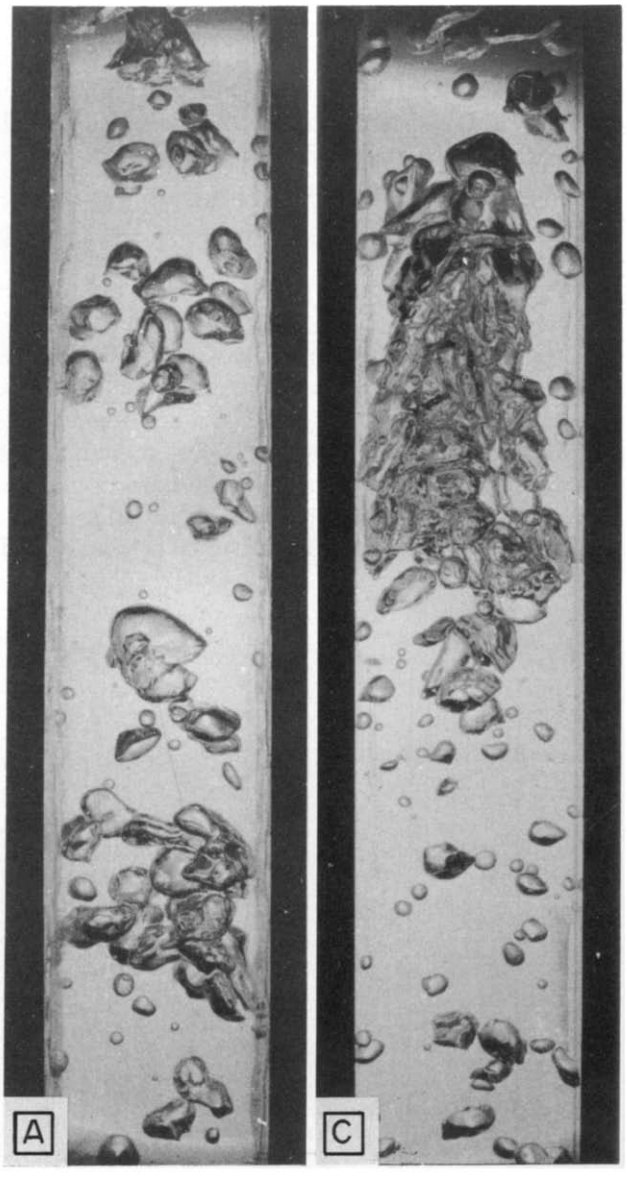

Figure 10b. An example of photo-shots at levels A and C; $j_L = 1.00$ m/s, $\langle \epsilon \rangle_A = 0.085$.

probability is embedded in a Lagrangian simulation of bubbly flow which helps us to create macroscopic modeling. Our experiments were performed with the intention of studying the large-scale structures of turbulent bubbly flow. For this reason, level A was chosen to represent already "fully developed void fraction profiles", provided that the bubble size was frozen. Level A was located in the experiment about $40D$ downstream from the bubble nozzle, which is larger than the scale of transverse lift towards the wall [$\sim 10D$ (Žun 1980)] but not enough for significant bubble coalescence at the chosen j_G. According to our observations and several other researchers (Serizawa 1974; Beyerlein *et al.* 1985), the distance of $40D$ downstream from the mixing chamber enables one to obtain a rather stable void fraction profile. What we are considering here, in contrast, is not the study of a "developing" profile downstream from the mixing chamber. We focus our attention on the evolution of an established void fraction profile into another shape on a much larger scale, i.e. $80D$ further from level A, when the interfacial conditions may be changed, which requires checking at least every $10D$ if this really happens. We therefore chose $5D$ as the lowest resolution in our deterministic assignment, which enabled us to rationalize the computing time.

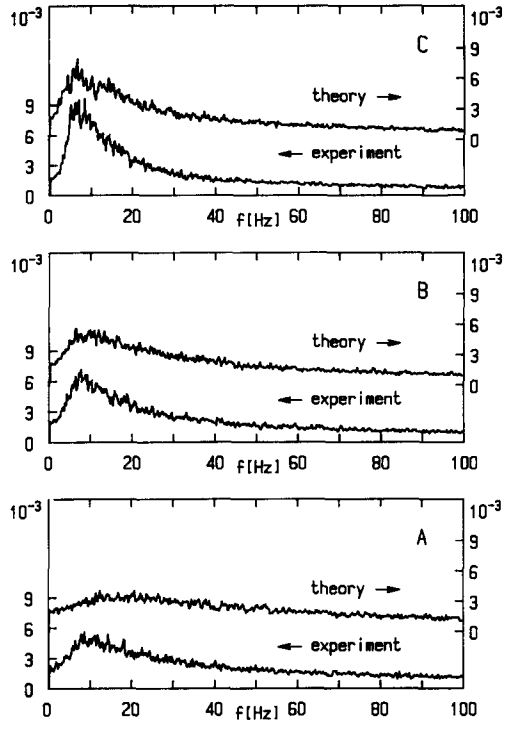

Figure 10c. Experimental and predicted PSDFs; $j_L = 1.00$ m/s, $\langle \epsilon \rangle_A = 0.085$.

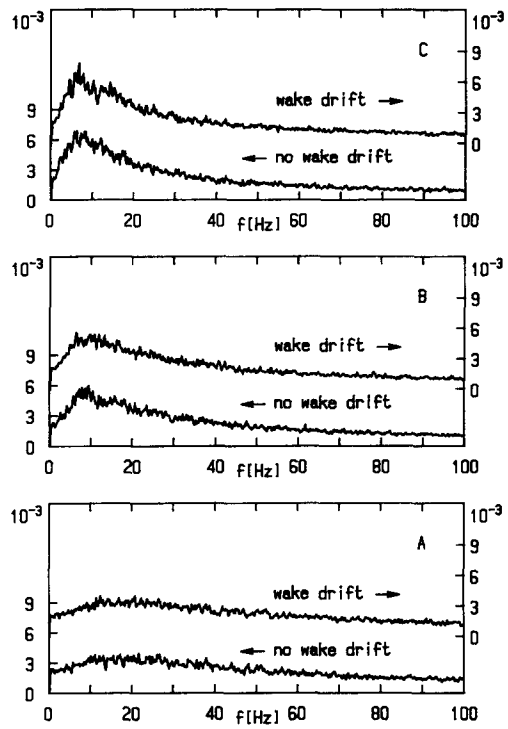

Figure 10d. Predicted PSDFs; *no wake drift*, $j_L = 1.00$ m/s, $\langle \epsilon \rangle_A = 0.085$.

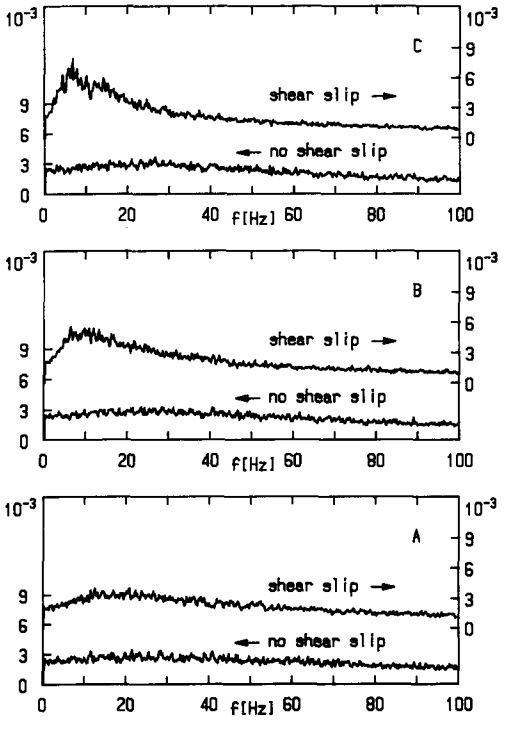

Figure 10e. Predicted PSDFs; *no shear slip*, $j_L = 1.00$ m/s, $\langle \epsilon \rangle_A = 0.085$.

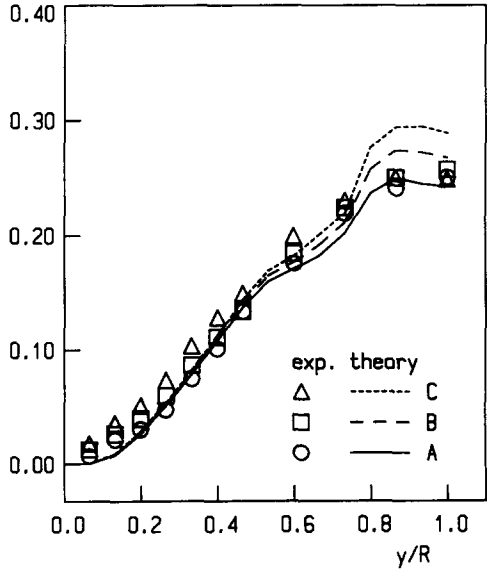

Figure 10f. Experimental and predicted void fraction profiles; $j_L = 1.00$ m/s, $\langle \epsilon \rangle_A = 0.085$.

Our intention here is to integrate the simulated flow of bubbles over fixed, non-sliding control volumes in the same manner as classical experiments to obtain the local void fraction and other statistically averaged data. What we expect from the comparison of simulated and experimental results is not a "generally valid model", as we believe this will never be achieved because of mixing effects and the nonisotropic nature of turbulence. What we would like is to learn something from the postulated dynamic processes on a micro-scale.

Local Time-averaged Void Fraction

The local void fraction was determined from the simulated bubbly flow process in the same way as for experimental signals. If a point (z_0, r_0) in the $(0 \leqslant z, 0 \leqslant r \leqslant R, \theta = 0)$ plane is observed at discrete time instants, a state density sequence $\psi_{z_0 r_0}(t_i)$ is formed by assigning the value 1 to instants when the point is occupied by the gas phase, and the value 0 to instants when the point is occupied by the liquid phase (Ishii 1975). ψ may be considered as a local instantaneous void fraction. The time-averaged void fraction at the point is obtained by averaging the sequence

$$\bar{c}(z_0, r_0) = \frac{1}{N} \sum_{i=0}^{N-1} \psi_{z_0 r_0}(t_i). \qquad [12]$$

Analysis of the Bubble Arrival Process

The frequency structure of the state density sequence may be analyzed using the discrete Fourier transform. The Fourier coefficients of a set consisting of N successive values $\psi(t_k)$, $k = 0, \ldots, N-1$, are obtained from

$$X_k = \Delta t \sum_{i=0}^{N-1} \psi(t_i) \exp(-j 2\pi i k / N), \qquad [13]$$

where Δt denotes the time interval between successive instants t_i. Each Fourier coefficient X_k corresponds to the frequency $k/N\,\Delta t$. The Nyquist criteria state that only coefficients from $k = 0$ to $k = N/2 - 1$ are meaningful (Bendat & Piersol 1986). The PSDF of the sequence ψ may then be calculated from the moduli of Fourier coefficients. This reveals the time structure (random or periodic) of the bubble arrival process and may lead to flow pattern identification. When one visually identifies a two-phase flow pattern or flow structure, one is limited to observing a tube section only a few internal diameters (or internal widths) long. If the length scale of the flow structure evolution is larger than the length of the section in which the structure is observed, the space structure of the frozen phase distribution along a fictional vertical chord which passes through the probe tip is analogous to the time structure of the probe signal. Thus, an analysis of the time periodicity of the bubble arrivals is also an analysis of the space periodicity of the flow structure. The evolution of the flow structure along the tube was observed by comparing the PSDFs obtained at the different vertical levels A, B and C.

Comments on Assumptions

This is the first time we have been able to follow the evolution of the bubbly-to-slug flow transition, but still only in a limited segment and based on some assumptions which are discussed below.

Flow symmetry

Flow symmetry relative to the $\theta = \pi/2$ plane.

Bubble shape, size and orientation

Rigid bubbles, ellipsoids or spherical caps, constant bubble size at level A, isothermal expansion, bubble symmetry axis always vertical; *a compromise in assuming constant bubble size results in some discrepancies in the void fraction profile in core region. This, however, does not have a significant effect on the pressure drop predictions one may obtain from the deposition model.*

Bubble and liquid velocity

Bubble relative velocity equal to terminal velocity, no inertial effects in bubble motion, undisturbed liquid velocity field: 1/7th profile, wake drift behind bubbles and bubble trains; *these assumptions appear to oversimplify the flow description. However, it was shown that in the case of a small-diameter tube, the wake drift does not contribute significantly to the bubble coalescence process. If the ζ value had been taken, for example, as 6 instead of 3, the results would have shown no significant difference. Similarly, there would be no major changes if k_t had been limited by 8 instead of 4 bubbles.*

Bubble interaction

Minimum relative overlapping necessary for bubble interaction: *to obtain significant differences, the change in s^*_{min} has to be of the order of ± 0.1. If the relative overlapping is not prescribed, the bubble clustering process is too fast.*

Bubble train definition: *the onset of the PSDF transition to periodic fashion is connected with the appearance of bubble train structures.*

Influence of liquid turbulence on bubble interaction: *in general, p_t increases the axial mobility of bubbles by assuming that bubble wobbling is intensified. This effect in combination with the resetting of the bubble rest time preserves independent bubble motion. To obtain significant changes, the variation of p_t has to be of the order of 0.1.*

Bubble rest time: *the bubble rest time is in direct proportion to the bubble coalescence rate and hence to the number density of larger bubbles. The evolution from a random towards a periodic structure is not necessarily affected by the value of the rest time.*

Instantaneous merging in wall region: *this does not have any effect on the void coring regimes, but is necessary to obtain the evolution from a wall void peaking into a void coring regime.*

Bubble segregation

Bubble deposition model: *this does not have any effect on the void coring regimes, but is necessary to obtain the evolution from a wall void peaking into a void coring regime.*

Probability of lateral migration: *at high void fraction, the change of P_s has to be of the order of ± 0.5 to obtain significant differences; at low void fraction, a value of P_s of the order of 1.0 almost completely prevents the evolution of the void fraction profile.*

6. CONCLUSIONS

The proposed Lagrangian/Eulerian simulation can serve as a possible bridge between microscopic understanding and macroscopic modeling. For the first time, the results of a direct simulation of the void peak evolution from the wall region to the tube core are presented for vertical flow.

The problem of scale separation in turbulent bubbly flow was analyzed. There are two principal deterministic processes going on simultaneously, namely bubble deposition and bubble coalescence. Each process runs on a different scale. Within the limits of the experiment, the bubble deposition takes about $10D$, whereas coalescence requires about $80D$. Fine-scale details can be taken into account by assigning the corresponding probabilities.

The theory deals with the crucial instability in the bubbly-to-slug flow transition, sharply localized in space and time. A simulation is proposed of the transition from nonhomogeneous, spatially random distributed bubbles into periodic bubbly structures. Two main kinematic characteristics of slug flow, no bubble lateral movement and the periodic appearance of the bubbles, seem to be reached long before the gas bubble takes up the whole tube cross-section. It seems that the coherent structures of bubbles traveling upwards in trains are formed with basically the same characteristics as for slug flow.

The key parameters at the bubbly-to-slug flow transition in the case of a wall void peaking flow regime seem to be: bubble transverse lift, bubble transverse dispersion and lateral penetration restraint, which determine bubble deposition or segregation; and, on the other hand, shear slip, wake drift and fluid–fluid interaction, which determine the bubble coalescence process.

Acknowledgements—Thanks are due to Mr M. Kljenak for the photography. Financial support was given by the Slovene Research Community.

REFERENCES

BENDAT, J. S. & PIERSOL, A. G. 1986 *Random Data—Analysis and Measurement Procedures*. Wiley, New York.

BEYERLEIN, S. W., COSSMAN, R. K. & RICHTER, H. J. 1985 Prediction of bubble concentration profiles in vertical turbulent two-phase flow. *Int. J. Multiphase Flow* **11**, 629–641.

BILICKI, Z. & KESTIN, J. 1987 Transition criteria for two-phase flow patterns in vertical upward flow. *Int. J. Multiphase Flow* **13**, 283–294.

ISHII, M. 1975 *Thermo-Fluid Dynamic Theory of Two-Phase Flow*, Eyrolles, Paris.

JONES, O. C. Jr. & ZUBER, N. 1975 The interrelation between void fraction fluctuations and flow patterns in two-phase flow. *Int. J. Multiphase Flow* **2**, 273–306.

KLJENAK, I. 1992 The transition from bubbly to slug flow. Doctoral Thesis, Faculty of Mechanical Engineering, Univ. of Ljubljana, Slovenia.

KLJENAK, I. & ŽUN, I. 1991 Computer simulation of bubble to slug flow transition in vertical tubes. In *Computational Methods and Experimental Measurements V* (Edited by SOUSA, A., BREBBIA, C. A. & CARLOMANGO, G. M.), pp. 285–296. CMP/Elsevier, Southampton/London.

MATUSZKIEWICZ, A., FLAMAND, J. C. & BOURÉ, J. A. 1987 The bubble–slug flow pattern transition and instabilities of void fraction waves. *Int. J. Multiphase Flow* **13**, 199–217.

OTAKE, T., TONE, S., NAKAO, K. & MITSUHASHI, Y. 1977 Coalescence and breakup of bubbles in liquids. *Chem. Engng Sci.* **32**, 377–383.

PRINCE, M. J. & BLANCH, H. W. 1990 Bubble coalescence and break-up in air-sparged bubble columns. *AIChE Jl* **36**, 1485–1499.

SERIZAWA, A. 1974 Fluid-dynamic characteristics of two-phase flow. Doctoral Thesis, Kyoto Univ., Japan.

SERIZAWA, A. & KATAOKA, I. 1990 Interfacial parameters in bubbly two-phase flow. Invited Paper presented at the *3rd Wkshp on CANDU and Advanced Reactor Thermohydraulics*, McMaster Univ., Hamilton, Ontario.

STUHMILLER, J. H., FERGUSON, R. E., WANG, S. S. & AGEE, L. J. 1983 Two-phase flow regime modeling. In *Transient Two-Phase Flow, Proc. 3rd CSNI Specialist Meeting* (Edited by PLESSET, M. S., ZUBER, N. & CATTON, I.), pp. 353–368. Hemisphere, Washington, DC.

THOMAS, R. M. 1981 Bubble coalescence in turbulent flows. *Int. J. Multiphase Flow* **7**, 709–717.

TSUCHIYA, K., MIYAHARA, T. & FAN, L.-S. 1989 Visualisation of bubble–wake interactions for a stream of bubbles in a two-dimensional liquid–solid fluidized bed. *Int. J. Multiphase Flow* **15**, 35–49.

WALLIS, G. B. 1975 The terminal speed of single drops or bubbles in an infinite medium. *Int. J. Multiphase Flow* **1**, 491–511.

ŽUN, I. 1980 The transverse migration of bubbles influenced by walls in vertical bubbly flow. *Int. J. Multiphase Flow* **6**, 583–588.

ŽUN, I. 1990 The mechanism of bubble non-homogeneous distribution in two-phase shear flow. *Nucl. Engng Des.* **118**, 155–162.

ŽUN, I., KLJENAK, I., SERIZAWA, A. & MOŽE, S. 1991 The evolution of bubble to slug flow transition. In *Phase Interface Phenomena in Multiphase Flow; ICHMT* (Edited by HEWITT, G. F., MAYINGER, F. & RIZNIĆ, J. R.), pp. 221–230. Hemisphere, Washington, DC.

ŽUN, I., KLJENAK, I. & SERIZAWA, A. 1992 Bubble coalescence and transition from wall void peaking to core void peaking in turbulent bubbly flow. In *Dynamics of Two-phase Flows* (Edited by JONES, O. C. & MICHIYOSHI, I.), pp. 233–249. CRC, Boca Raton, FL.